NeuroImage 93 (2014) 138–145

Contents lists available at ScienceDirect

NeuroImage

journal homepage: www.elsevier.com/locate/ynimg

Are glutamate and lactate increases ubiquitous to physiological activation? A ^{1}H functional MR spectroscopy study during motor activation in human brain at 7 Tesla

Benoît Schaller [a,*], Lijing Xin [b], Kieran O'Brien [c], Arthur W. Magill [a,b], Rolf Gruetter [a,b,d,**]

[a] Laboratory of Functional and Metabolic Imaging, Ecole Polytechnique Federale de Lausanne, Station 6, 1015 Lausanne, Switzerland
[b] Department of Radiology, University Hospitals of Lausanne Rue du Bugnon 21, 1011 Lausanne, Switzerland
[c] Centre d'Imagerie BioMédicale, University of Geneva, Geneva 14, Geneva, Switzerland
[d] Department of Radiology, University Hospitals of Geneva, Rue Gabrielle-Perret-Gentil 4, 1211 Geneva 14, Switzerland

ARTICLE INFO

Article history:
Accepted 10 February 2014
Available online 18 February 2014

Keywords:
Lactate
Oxidative metabolism
Motor stimulation
^{1}H MR spectroscopy
Cerebral metabolic rate
Neurotransmitter
Glutamate

ABSTRACT

Recent studies at high field (7 Tesla) have reported small metabolite changes, in particular lactate and glutamate (below 0.3 μmol/g) during visual stimulation. These studies have been limited to the visual cortex because of its high energy metabolism and good magnetic resonance spectroscopy (MRS) sensitivity using surface coil. The aim of this study was to extend functional MRS (fMRS) to investigate for the first time the metabolite changes during motor activation at 7 T. Small but sustained increases in lactate (0.17 μmol/g ± 0.05 μmol/g, $p < 0.001$) and glutamate (0.17 μmol/g ± 0.09 μmol/g, $p < 0.005$) were detected during motor activation followed by a return to the baseline after the end of activation. The present study demonstrates that increases in lactate and glutamate during motor stimulation are small, but similar to those observed during visual stimulation. From the observed glutamate and lactate increase, we inferred that these metabolite changes may be a general manifestation of the increased neuronal activity. In addition, we propose that the measured metabolite concentration increases imply an increase in ΔCMR_{O2} that is transiently below that of ΔCMR_{Glc} during the first 1 to 2 min of the stimulation.

Introduction

Functional MR spectroscopy (fMRS) provides direct insights into brain metabolism by investigating the metabolic response of the brain to a physiological stimulus. The high spectral resolution and signal-to-noise ratio (SNR) of fMRS at high field (>3 Tesla) improve the accuracy and precision of the quantification of many brain metabolites (Mekle et al., 2009; Tkac et al., 2001, 2009). In addition to the increased chemical shift dispersion, a high time resolution is of advantage for the characterization of the small transient changes observed. Recent fMRS studies (Lin et al., 2012; Mangia et al., 2007b; Schaller et al., 2013) at high field (7 Tesla) reported small metabolite concentration changes during visual stimulation (around 0.2 μmol/g). In particular, a very small lactate concentration increase between 10 and 23% has been observed. Recently, functional diffusion-weighted MRS has been used to investigate metabolite ADC changes as a potential consequence of micro structural changes during activation (Branzoli et al., 2013).

The lactate increase observed during visual stimulation has been suggested to explain the mismatch of cerebral metabolic rate of change for glucose (ΔCMR_{Glc}) (or cerebral blood flow, CBF) and cerebral metabolic rate of change for oxygen (ΔCMR_{O2}) during brain activation. However, many studies have reported different results concerning the transient mismatch of ΔCMR_{Glc}, CBF and ΔCMR_{O2} during functional activity (reviewed in Buxton (2010)). The characterization of these changes has been reported in positron emission tomography (PET) (Fox and Raichle, 1986; Fox et al., 1988; Fujita et al., 1999; Marrett and Gjedde, 1997; Vafaee and Gjedde, 2000) and in MR studies (Chen et al., 1993, 2001; Davis et al., 1998; Hoge et al., 1999; Kim and Ugurbil, 1997; Kim et al., 1999; Lin et al., 2010; Liu et al., 2004; Vafaee et al., 2012; Wey

Abbreviations: Asp, aspartate; Cerebral metabolic rate, CMR; CRLB, Cramér–Rao lower bounds; Cr, creatine; tCho, total choline; FASTMAP, fast automatic shimming technique by mapping along the projections; Functional magnetic resonance imaging, fMRI; Functional magnetic resonance spectroscopy, fMRS; GABA, γ-aminobutyric acid; Gln, glutamine; Glu, glutamate; GSH, glutathione; Ins, myo-inositol; Lac, lactate; tNAA, total NAA; NAA, N-acetylaspartate; NAAG, N-acetylaspartylglutamate; NT, number of transients; OVS, outer volume suppression; PCr, phosphocreatine; PE, phosphoryl-ethanolamine; Signal-to-noise, SNR; SPECIAL, spin echo full intensity acquired localized; SNR, signal-to-noise ratio; Tau, taurine; VAPOR, variable power RF pulses with optimized relaxation delays; VOI, volume of interest; WS, water suppression.

* Corresponding author.
** Corresponding author at: Ecole Polytechnique Federale de Lausanne, SB-IPMC-LIFMET, Station 6, 1015 Lausanne, Switzerland. Fax: +41 21 693 79 60.
E-mail addresses: benoit.schaller@cardiov.ox.ac.uk (B. Schaller), lijing.xin@epfl.ch (L. Xin), kieran.obrien@epfl.ch (K. O'Brien), a.magill@fz-juelich.de (A.W. Magill), rolf.gruetter@epfl.ch (R. Gruetter).

http://dx.doi.org/10.1016/j.neuroimage.2014.02.016
1053-8119/

et al., 2011), and their differences have been attributed to different experimental conditions and the brain region examined (Buxton, 2010; Rothman et al., 2003; Vafaee and Gjedde, 2000, 2004; Zhu et al., 2009). Nevertheless, an energy balance calculation suggests that the energy demands during visual activation are largely met through oxidative metabolism at all times (Mangia et al., 2007a).

A positive BOLD signal appears to be a universal hallmark of physiological brain activation and has been suggested to depend on a mismatch ratio between cerebral blood flow change (ΔCBF) and ΔCMR_{O2}, the magnitude of which remains undetermined (reviewed in Buxton (2010)). Metabolite changes detected with fMRS likely reflect changes through oxidative and non-oxidative pathways.

Therefore, the aim of this study was to determine the metabolite changes occurring during motor activation in the human brain and to analyze the changes in terms of BOLD effect and relative CMR_{O2} and CMR_{Glc} changes.

Materials and methods

Subjects

Eleven healthy subjects (9 men and 2 women aged 18 to 26 years, right-handed) were enrolled in the fMRS study. One additional subject was used in a preliminary study to investigate the effect of the dielectric pad. All the subjects gave informed consent according to the procedure approved by the local ethics committee. The experiments were performed on a 7 T/68 cm scanner (Siemens, Erlangen, Germany) with the use of a single-channel quadrature transmit (physical z length ~180 mm) and 32-channel receive coil (Nova Medical Inc., MA, USA).

Dielectric pad

A single MR-invisible dielectric pad was constructed as specified in Teeuwisse et al. (2012a). The pad measured 100 × 100 × 5 mm^3 and was filled with a solution of deuterated water and barium titanate (dielectric permittivity of 160). The dielectric pad was placed directly on the subject's head, above the central sulcus of the left hemisphere. Full wave electromagnetic simulations were executed with Microwave Studio (CST, Darmstadt, Germany) to study the RF field distribution and the corresponding SAR maps. The simulated coil was loaded with a human head model (Duke from the Virtual Family (Christ et al., 2010)) and run with and without the dielectric pads present (same position as in the fMRS experiment). Subsequently, B_1^+ maps were acquired for one volunteer using the SA2RAGE sequence (TR = 2400 ms, TE = 0.78 ms, TD_1 = 45 ms, TD_2 = 1800 ms, $\alpha_1 = 4°$, $\alpha_2 = 10°$, 2 × 2 × 2.5 mm^3 resolution and a 128 × 128 × 64 matrix size acquired with sagittal orientation, TA = 1 min 55 s, reference voltage = 170 V) (Eggenschwiler et al., 2011), with and without the dielectric pad present.

Activation paradigm

During the functional MRS runs, the subject was asked to execute a cued finger-to-thumb tapping task with both hands at a frequency of 3 Hz. Subjects were asked to execute a demanding motor task at a finger-tapping rate of 3 Hz, which elicits the highest changes for CBF (which occurs in parallel to CMR_{Glc} (Gjedde et al., 2002; Paulson et al., 2010)) and CMR_{O2} in the primary motor cortex (Vafaee and Gjedde, 2004). The tip of each finger was applied twice to the thumb for each hand. The bilateral finger-to-thumb movement was repeated during the entire activation period. Numbers from 1 to 4 (one number was associated to each finger) were projected on a screen at the back of the scanner to provide the visual cue. During the rest period, the subject was asked to keep his hands in the same position (palms open) and not to move his fingers. Proper understanding and good performance of the activation paradigm (rate, amplitude and intensity of the finger-tapping) was guaranteed by a practice session outside the scanner beforehand. While performing the task in the scanner during the experiment, subject's performance was carefully monitored. Foam padding was placed around the head of the participants to ensure the subject's comfort and to minimize motion. During the fMRS measurement, each subject performed the motor task with the following timing: four alternate periods of 5 min of motor activation and rest (ON–OFF–ON–OFF), preceded by a 2 min rest period (22 min total duration).

MR protocol

Anatomical images were acquired using MP2RAGE (Marques et al., 2010) (TR = 5500 ms, TE = 2.84 ms, TI_1 = 750 ms, TI_2 = 2350 ms, $\alpha_1 = 4°$, $\alpha_2 = 5°$, 1 × 1 × 1 mm^3 resolution, 256 × 256 × 176 matrix size acquired with sagittal orientation and TA = 7 min 20 s). A "localizer" fMRI experiment was performed (20 s ON, 20 s OFF, total acquisition time of 2 min 30 s, previously described motor task) using a multi-slice EPI sequence similar to the one described in van der Zwaag et al. (2009). The overlap of the activation map on the anatomical images guided the placement of the voxel of interest (VOI) for the subsequent fMRS scans. The VOI was placed in an area of high motor activation, covering the hand area of the motor and the somatosensory cortices (inset in Fig. 3). First- and second-order shims were adjusted using FAST(EST)MAP (shim volume = 22 × 25 × 22 mm^3) (Gruetter, 1993; Gruetter and Tkac, 2000). Flip angles of the water suppression pulses were optimized to reduce the residual water peak height below that of NAA. In addition, OVS bands were carefully placed to suppress signal from outside the VOI, in particular extra cerebral fat signal. ^{1}H MR spectra were continuously acquired during the functional task using the semi adiabatic SPECIAL sequence (TR/TE = 7500/12 msec, bandwidth = 4000 Hz, vector size = 2048 pts, VOI = 17 × 20 × 17 mm^3, NT = 88 × 2) (Xin et al., 2012) preceded by VAPOR water and outer volume suppression (Tkac and Gruetter, 2005).

Data processing

Free induction decay (FID) signals were acquired for each pair of scans (NT = 2). The individual ^{1}H MR spectra were frequency corrected using home-written Matlab (Mathworks, Natick, MA, USA) routine to compensate for small B_0 drift (Tkac and Gruetter, 2005) by aligning the creatine peak (3.03 ppm) of ^{1}H MR spectra. ^{1}H MR spectrum time courses were first analyzed in single subjects by averaging spectra in blocks of 4 spectra. To validate the metabolite changes, a paired two-tailed student *t*-test was performed based on the individual time courses of each subject. In a second approach (group analysis), FIDs were averaged over the eleven subjects in blocks of 22 ^{1}H MR spectra (2 spectra per subject, n = 11). A moving average with kernel of 4 points was used to plot the time courses.

To further validate the observed metabolite changes, the ^{1}H MR spectra from the last 3.75 min of each period were summed separately between activation (NT = 56, n = 11) and rest (NT = 56, n = 11) and then subtracted to yield a difference spectrum. To validate the statistical significance of the metabolite changes, a paired two-tailed student *t*-test was performed using the quantification of the aforementioned summed activation spectra and the summed rest spectra for each subject. Metabolite changes with p-values below 0.05 were considered to be statistically significant. The transition time of the hemodynamic response at the beginning of a period (rest or activation) was not considered, neither for the statistical analyses, nor for the difference spectrum, as the metabolites had not reached yet their respective new steady state. The BOLD effect correction of the difference spectrum was performed by applying an additional line-broadening (lb = 0.25 Hz) to the summed activation spectra. The correction implied the minimization of the Cr (3.03 ppm) and NAA (2.01 ppm) resonances in the difference spectrum.

All ^{1}H MR spectra and difference spectra were fitted and quantified using LCModel (Provencher, 1993) with a basis set of simulated spectra of 20 metabolites using published values for chemical shift and

J-coupling (Govindaraju et al., 2000; Xin et al., 2008). A macromolecule signal measured in predominantly gray matter was also included in the basis set. The LCModel analysis was carried out from 0.2 to 4.2 ppm. A creatine concentration of 8 μmol/g was assumed for the scaling of the metabolite concentrations. Only metabolites with Cramér–Rao lower bounds (CRLB) below 30% were used for statistical analysis (NT = 56) and for the group analysis (NT = 22). For the individual time courses (NT = 4), lactate and glutamate were quantified with CRLB below 40%.

Results

To mitigate the limitations imposed on B_1^+, a dielectric pad was placed above the central sulcus (left hemisphere) in order to shift the B_1^+ "hot spot" towards the area of interest at the expense of decreasing the B_1^+ intensity in the lower parts of the brain (frontal lobe and visual cortex). Simulations of the RF field distribution were run without and with the pad present (data not shown) and no increase of the peak local 10 g-averaged SAR was observed, in agreement with previous reports (Snaar et al., 2011; Teeuwisse et al., 2012a,b).

To investigate the benefit of using a dielectric pad, B_1^+ maps were acquired with one volunteer without and with the pad present (Fig. 1A, left and middle images). The presence of the pad enabled a B_1^+ sensitivity gain up to 50% in the area of interest under investigation on B_1^+ maps (Fig. 1A, right).

First- and second-order shims resulted in typical water linewidths of 12.6 ± 0.8 Hz (mean ± SD, n = 11). Stable and reproducible ^{1}H MR spectra with negligible lipid contamination were acquired during the fMRS experiment (Fig. 1B) and the SNR of N-acetylaspartate (NAA) resonance was typically 57 ± 5 (mean ± SD, n = 11) for a pair of scans. The water signal was generally minimized below the height of the NAA peak and no signal contamination, due to extraneous lipid, was observed in the spectral region 1–2 ppm.

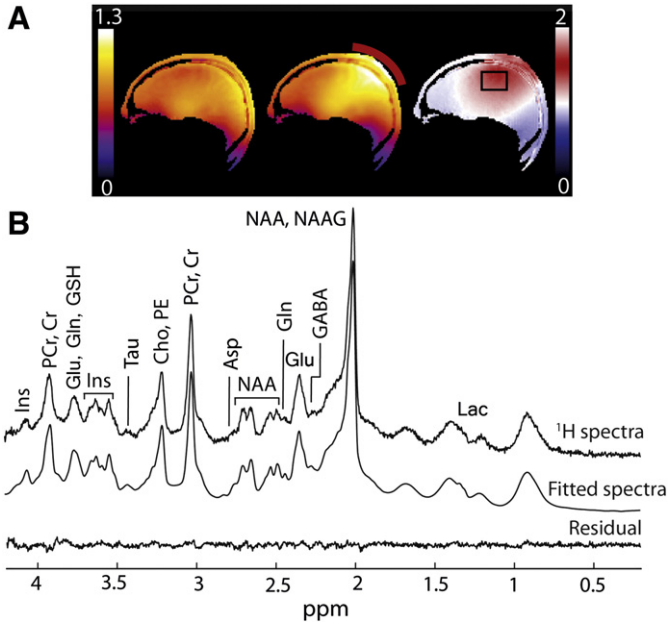

Fig. 1. (A) Improved transmit B_1 for localized MRS using a dielectric pad (red bar in the middle image). Measured B_1^+ maps without (left) and with (middle) the dielectric pad present. The ratio of the two images (right) shows a B_1^+ increases up to twice in the area of interest (black square), above which the pad was placed. The scale of the B_1^+ maps, obtained using SA2RAGE sequence (Eggenschwiler et al., 2011) corresponds to a multiplicative factor of a desired flip angle. (B) Representative ^{1}H MR spectra acquired with semi-adiabatic SPECIAL sequence (TR/TE = 7500/12 ms, bandwidth = 4000 Hz, vector size = 2048 pts, VOI = 17 × 20 × 17 mm^3, NT = 22) and the dielectric pad. 8 metabolites were reliably quantified with LCModel with CRLB below 10%: creatine (Cr), phosphocreatine (PCr), glutamine (Gln), glutamate (Glu), myo-inositol (Ins), N-acetylaspartate (NAA), N-acetylaspartylglutamate (NAAG) and total choline (tot Cho); 5 metabolites with CRLB below 20%: aspartate (Asp), γ-aminobutyrate (GABA), glutathione (GSH), lactate (Lac), and taurine (Tau); and 1 metabolite with CRLB less than 30%: and Phosphoethanolamine (PE).

To determine that the placement of the VOI minimized partial volume effect, the influence of the physiological activation on the ^{1}H MR spectra linewidth was investigated. In particular, the creatine peak height was measured to assess the metabolite BOLD effect. Linewidth narrowing of the ^{1}H MR spectra, which is induced by the BOLD effect (Zhu and Chen, 2001), was observed during the time course (data not shown) and resulted in a mean increase of the creatine peak height of 2% during activation periods (n = 11).

To investigate the metabolite changes for individual subjects, the ^{1}H MR spectra were first averaged in blocks of 4 spectra. Lactate (Lac) and glutamate (Glu) were quantified with CRLB below 40% and 5%, respectively. The mean variation of the Lac and Glu concentrations of the averaged time courses was below 0.05 μmol/g and 0.07 μmol/g, respectively, for both periods (rest and activation), well below the observed metabolite increases. Statistically significant increases of Lac by 17 ± 5% (0.17 ± 0.05 μmol/g, $p < 0.001$, n = 11) and of glutamate (Glu) by 2 ± 1% (0.17 ± 0.09 μmol/g, $p < 0.005$, n = 11) were found when comparing the quantification of the summed activation spectra to the summed rest spectra (NT = 56 for given activation and rest periods) (Table 1). No other metabolite changes reached statistical significance.

To analyze the metabolite changes, ^{1}H MR spectra were averaged between the subjects by blocks of 22 spectra (group analysis, n = 11), which enabled a native time resolution of 15 s for the metabolite time courses (Fig. 2A). The averaged ^{1}H MR spectra allowed quantification of 8 metabolites with CRLB less than 10% (creatine, phosphocreatine, glutamine, glutamate, myo-inositol, N-acetylaspartate, N-acetylaspartylglutamate and total choline), 5 metabolites with CRLB less than 20% (aspartate, ϒ-aminobutyrate, glutathione, lactate, and taurine) and 1 metabolite (Phosphoethanolamine) with CRLB less than 30%. Note that the plots with the moving average (Fig. 2B) indicated that a steady state was reached by Lac and Glu within the first 1–2 min of activation.

To confirm the observed metabolite changes, a difference spectrum was obtained by subtracting the summed rest spectra (NT = 56, n = 11) to the summed activation spectra (NT = 56, n = 11) (Figs. 3A–C). The linewidth narrowing caused by the BOLD effect was clearly visible in the difference spectrum at the singlet resonances of Cr (3.03 ppm) and NAA (2.01 ppm). Therefore, an additional line-broadening of 0.25 Hz was applied to the summed spectra acquired during activation to correct for the linewidth narrowing, resulting in a detectable Glu and Lac increases at 2.1/2.3/3.7 ppm and 1.3/4.1 ppm, respectively (Fig. 3D). LCModel quantification of the corrected difference spectrum provided Lac and Glu increases of 0.19 ± 0.01 μmol/g and 0.10 ± 0.01 μmol/g (concentration ± CRLB), respectively (Fig. 3E).

Table 1
Mean lactate (Lac) and glutamate (Glu) concentrations during the rest or activation periods and the concentration changes during the functional paradigm. Only Lac and Glu changes were significant ($p < 0.05$, paired two tailed *t*-test). The mean concentration for the rest and activation periods (μmol/g) were obtained from the summed activation and rest spectra (NT = 56 scans for rest and for activation periods, n = 11). Concentration changes are expressed in absolute concentration (μmol/g) or in percentage (%). Data are expressed as mean ± s.e.m.

	Metabolite concentration at rest (μmol/g)	Metabolite concentration during activation (μmol/g)	Concentration change	
			Absolute (μmol/g)	Percentage (%)
Lac	1.02 ± 0.03	1.20 ± 0.03	0.17 ± 0.05	17 ± 5
Glu	10.25 ± 0.06	10.41 ± 0.06	0.17 ± 0.09	2 ± 1

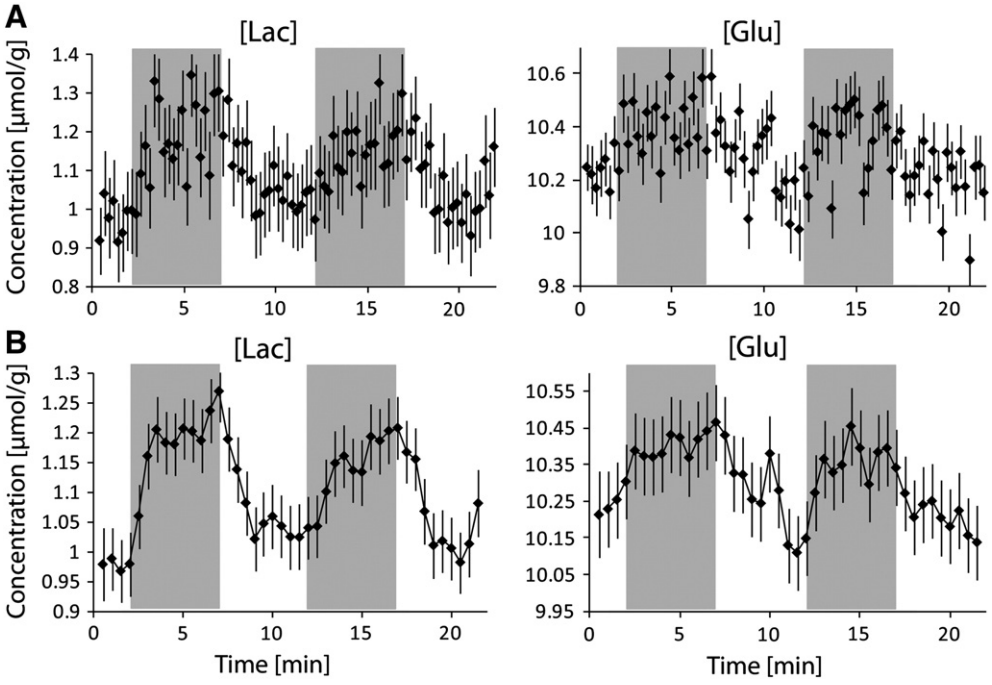

Fig. 2. (A) Group analysis shows the time courses of Lac and Glu during the functional paradigm with a time resolution of 15 s. Each time point is the averaged of 22 ^{1}H MR spectra (2 scans per subject, n = 11). (B) A moving average was applied after quantification (moving average kernel of 4 scans). Data are reported as mean ± s.e.m. in µmol/g.

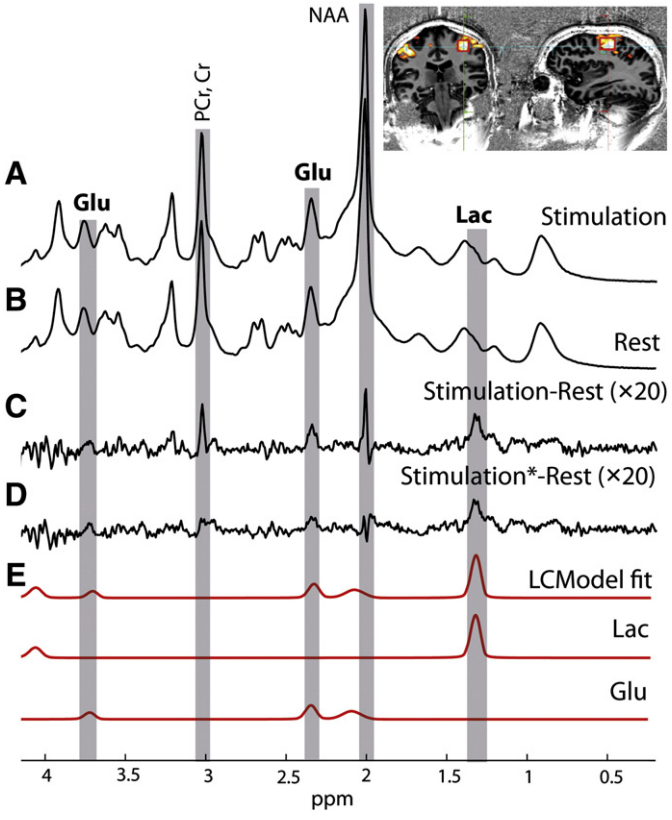

Fig. 3. Summed ^{1}H spectrum acquired during activation (A) and rest (B) periods (NT = 56, n = 11). Subtraction of the summed rest spectra to the summed activation spectra provided the difference spectrum (C). An additional line broadening (*) of 0.25 Hz was applied to the summed activation spectra to correct for the BOLD effect on metabolite linewidth (D). LCModel quantification of the corrected difference spectrum (E) yielded a Lac and Glu increase of 0.19 ± 0.01 µmol/g and 0.10 ± 0.01 µmol/g (concentration ± CRLB), respectively. A line broadening of 1 Hz was applied to all the ^{1}H MR spectra. Inset: Overlap of the anatomical image and the activation map. The location of the VOI (17 × 20 × 17 mm^3) covering the motor and somatosensory cortices is indicated by a red square.

Discussion

This study reports metabolite changes in the human brain during motor activation. A lactate increase of 17 ± 5% ($p < 0.001$) and a glutamate increase of 2 ± 1% ($p < 0.005$) were observed during the activation periods (Table 1). The magnitude of the observed metabolite changes is comparable to previous reports performed in the visual cortex (Lin et al., 2012; Mangia et al., 2007a; Schaller et al., 2013).

The use of the semi adiabatic SPECIAL sequence (Xin et al., 2012) at 7 T and the dielectric pad (Fig. 1A) yielded sufficient sensitivity to investigate the metabolite changes during motor activation, as judged from CRLB of Lac and Glu with CRLB < 12% and 2% (NT = 22), respectively (Fig. 1B). Based on the fMRI "localizer" experiment, the VOI was placed in an area of intense motor activation. ^{1}H MR spectra were devoid of any potential lipid contamination in the region 1–2 ppm. The increase of the creatine peak height (approximately 2%) during the activation periods gave evidence that the VOI was placed in the activated area (data not shown). From the individual times courses, lactate increases were noticeable in each subject, but the change was more apparent when averaging across all subjects. In addition to Lac, a Glu increase was also observed during activation and both increases were confirmed by the group analysis (Fig. 2). The plots of the metabolite changes of the group analysis clearly illustrated a new steady state reached by the metabolites. These observations and the magnitude of the changes were comparable to those reported by previous studies during visual stimulation at 7 T (Lin et al., 2012; Mangia et al., 2007b; Schaller et al., 2013). LCModel quantification of the difference spectrum (Fig. 3), corrected for the BOLD narrowing of the linewidth during activation, yielded Lac and Glu increases, which were consistent with the metabolite changes observed in the group analysis.

A lactate increase of 0.17 ± 0.05 µmol/g ($p < 0.001$, n = 11) was observed upon motor stimulation in this study and a new steady state was reached within the first minutes of activation (Fig. 2). As discussed by Mangia et al. (2007a), the increase in Lac, which implies an increase in pyruvate (Pyr) (because of the dynamic equilibrium between Lac and Pyr), may sustain the increased flux into the oxidative pathway by stimulating the activation of pyruvate dehydrogenase (Hawkins et al.,

1973). The steady state may reflect a balance between Lac production and Lac efflux to the blood, as suggested by (Mangia et al. (2007a).

Many studies have reported different lactate changes in the two last decades during visual activation: an increase of 10–250% (Frahm et al., 1996; Prichard et al., 1991; Sappey-Marinier et al., 1992) or the absence of changes (Boucard et al., 2005; Merboldt et al., 1992; Sandor et al., 2005). Kuwabra et al. reported a large lactate increase during motor stimulation in the basal ganglia at 1.5 T (mean increase of Lac/Cr of 0.2) (Kuwabara et al., 1995). In addition to an optimized methodology, increases of chemical shift dispersion, spatial and temporal resolutions at high field are crucial for an accurate and reliable quantification of the metabolite changes. Recent studies, performed at 7 T (Lin et al., 2012; Mangia et al., 2007a; Schaller et al., 2013), reported consistent increases of lactate during visual stimulation (10–20%). However, in contrast to Lin et al., which showed a transient increase of Lac during activation, both Mangia et al. (2007a) and Schaller et al. (2013) observed an increase of Lac to a new steady state within the first 1–2 min of visual activation similar to that observed in this study during motor activation.

Additionally, an increase of Glu of 0.17 ± 0.09 μmol/g ($p < 0.005$, $n = 11$) was observed during the motor activation similar to that was detected in visual stimulation (Schaller et al., 2013). Several factors have been suggested to explain the Glu changes during activation (reviewed in Mangia et al. (2012)) such as an increased flux through the malate–aspartate shuttle (Mangia et al., 2007a; McKenna et al., 2006), increased Glu/Gln cycling, or GSH synthesis (Lin et al., 2012). In addition to the Asp decrease already reported by Mangia et al., and Lin et al. reported a significant change for GSH, which may support these hypotheses. However, neither Asp nor GSH significantly changed in our study. Therefore, the Glu change observed was likely generated by increased flux through pyruvate carboxylase (Oz et al., 2004) and via glutamate dehydrogenase (McKenna et al., 2000) (Fig. 4B).

Unlike Mangia et al. (2007a) and Lin et al. (2012), Glc and Asp concentration changes were not significant in this study and no trends were observed on the time courses.

It is of interest to note that the lactate increase observed during motor activation (17 ± 5%) was similar to that observed during visual activation (19 ± 4%) (Schaller et al., 2013). However, the Glu change was halved when comparing the motor activation (2 ± 1%) to the visual activation (4 ± 1%). Meanwhile, motor activation also led to a similar reduction in BOLD response as detected with the creatine peak height percentage change (2% in the motor activation versus 3% in the visual activation) and by the BOLD effect correction applied to the summed activation spectra (line broadening of 0.25 Hz in the motor activation versus 0.45 Hz in the visual activation (Schaller et al., 2013)). While a proportional relationship may exist between the increased flux through oxidative pathways and change in BOLD response (Davis et al., 1998; Hoge et al., 1999; Lin et al., 2010), this also suggest that partial volume effect might lead to reduced Glu changes, even though a small VOI ($17 \times 20 \times 17$ mm^3) was used in this study.

Although Mangia et al. (2007a) concluded from similar lactate increase that energy demands at steady state are nearly completely matched by oxidative energy metabolism, they also noted that this may not be the case throughout the entire time course. The small increase in glutamate and lactate likely imply a small transient mismatch of glucose and oxygen metabolic rates, as they represent an increment in carbons in tissue (not being oxidized).

In the following, we provide an estimate of implied CMR_{O2} and CMR_{Glc} changes noting that the relative change in CMR_{Glc} over CMR_{O2} may very well be smaller, as the changes may not account for all CMR_{O2} changes.

Changes in glucose ($\Delta CMR_{Glc(tot)}$) and oxygen metabolism (ΔCMR_{O2}) can be inferred from the initial rise of lactate and glutamate, as follows: we estimate that steady-state levels of lactate and glutamate are reached approximately 1.5 min after onset of stimulation, resulting in a net increase of carbon in tissue, otherwise metabolized to CO_2. The rate of lactate increase thus amounts to approximately 0.11 μmol/g/min, which corresponds to a non-oxidative glucose consumption, $\Delta CMR_{Glc,non\text{-}ox}$, of approximately 0.06 μmol/g/min by glycolysis (Fig. 4A). The glutamate rate increase by approximately 0.11 μmol/g/min is likely the result of increased flux through pyruvate carboxylase (PC) (Oz et al., 2004), which in turn implies an oxidative glucose consumption, $\Delta CMR_{Glc,ox}$, of 0.11 μmol/g/min to complete a 6-carbon molecule (citrate) (Fig. 4B). Thus, the total increase of glucose consumption during the stimulation, $\Delta CMR_{Glc(tot)}$, was estimated at 0.17 μmol/g/min, which corresponds to a 40–50% increase from the basal state of CMR_{Glc} (0.34–0.42 μmol/g/min (Alkire et al., 1999; Huisman et al., 2012)). It is of interest to note that such estimated $\Delta CMR_{Glc(tot)}$ is close to ΔCBF reported in previous PET studies during motor stimulation (Ito et al., 2005) or somatosensory stimulation (Fox and Raichle, 1986), but $\Delta CMR_{Glc(tot)}$ may actually exceed the estimated value due to incremental CMR_{O2} not accounted for by this calculation.

To determine the relative increase of ΔCMR_{O2} during activation, the contribution of the ATP production coupled to mitochondrial oxidation,

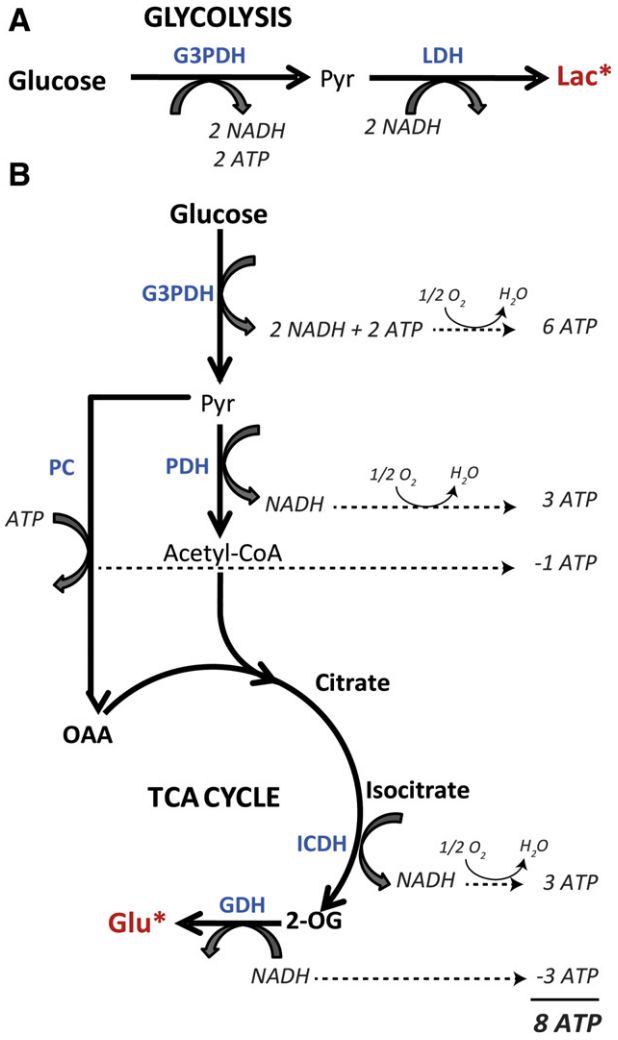

Fig. 4. Proposed scheme illustrating changes of glucose consumption (ΔCMR_{Glc}) associated with the observed metabolite changes of Lac and Glu (red*) occurring during neuronal motor activation. Lactate (Lac) increase is generated by anaerobic glycolysis (A) whereas glutamate (Glu) changes may be achieved through pyruvate carboxylation (PC), a reaction requiring oxygen consumption (B). A total increase of the glucose consumption, $\Delta CMR_{Glc(tot)}$, of 40–50% and relative increase of oxygen consumption (from ATP consideration), ΔCMR_{O2}, of 8% were inferred from the initial rise of Lac and Glu time courses (see Discussion). G3PDH, glyceraldehyde-3-phosphatedehydrogenase; LDH, lactate dehydrogenase; PDH, pyruvate dehydrogenase; ICDH, isocitrate dehydrogenase; GDH, glutamate dehydrogenase, 2-OG, alpha-ketoglutarate.

relative to the glucose used for glutamate synthesis ($\Delta CMR_{Glc,ox}$ = 0.11 μmol/g/min) was evaluated: not all glucose that enters the TCA cycle from pyruvate will be completely oxidized and thus will not deliver 36 ATPs per glucose from the produced NADH and $FADH_2$, which can be seen as follows: the synthesis of one citrate from oxaloacetate (OAA) and Acetyl-CoA requires 2 molecules of pyruvate (1 through PC and 1 through pyruvate dehydrogenase) (Fig. 4B). The produced NADH is oxidized via the electron transport chain and hence energy results in ATP synthesis. The synthesis of glutamate from glucose produces 8 ATPs instead of the 36 ATPs for complete oxidation of glucose, thereby consuming considerably less O_2 per glucose molecule (i.e. 8/36 of O_2 normally required for complete glucose oxidation). When assuming a near-complete oxidation of glucose at rest (Siesjo, 1978), the oxidation of $\Delta CMR_{Glc,ox}$ leading to glutamate increase corresponds to ΔCMR_{O2} of $5.5 \times \Delta CMR_{Glc,ox} \times 8/36 = 0.14$ μmol/g/min, which amounts to a relative ΔCMR_{O2} increase of 10% (given a basal state of 1.5 μmol/g/min (Ito et al., 2005)). Note that this incremental ΔCMR_{O2} is close to the reported CMR_{O2} increase in motor stimulation (Ito et al., 2005) and somatosensory stimulation (Fox and Raichle, 1986). In addition, a recent study by Vafaee et al. (2012) reported a ΔCMR_{O2} ~6% after 1 min of finger tapping activation in M1 motor area.

The phosphocreatine pool is a high energy reserve in the brain. However, with the high number of ATP produced per glucose molecule, the effect of a 10% PCr reduction in the first minute (which is possible within experimental error), results in approximately 0.3 μmol/g/min ATP produced (given a basal state of 0.3 μmol/g/min (Mekle et al., 2009)), a quantity that is negligible in the overall energy budget.

It is important to stress that the estimated changes in ΔCMR_{Glc} and ΔCMR_{O2} were calculated by neglecting any concomitant increase in $\Delta CMR_{Glc,ox}$ not detected by the metabolite changes. However, such an additional increment in $\Delta CMR_{Glc,ox}$ does not alter the conclusion of a transient mismatch, as can be seen from the following example: adding a 10% increase in ΔCMR_{Glc} and ΔCMR_{O2} yields a $\Delta CMR_{Glc(tot)}$ of 50–60% and a ΔCMR_{O2} of 20%. Note, however, that it is equally likely that increased metabolism during activation results in an increase of glycolytic and TCA cycle intermediates, derived from glucose and thus not completely oxidized.

Therefore, within the experimental errors of the present study, the metabolic changes in the first minutes imply a transient drop in oxygen–glucose index (OGI), defined as the molar ratio of oxygen consumption to glucose utilization CMR_{O2}/CMR_{Glc} (OGI = 6 if glucose is completely oxidized). It is thus plausible that the measured changes mainly represent the metabolic events during the first minutes of the PET studies, given the characteristics of the bolus-shaped arterial input function of PET FDG studies and the short half-life of 2 min of ^{15}O (Fox and Raichle, 1986; Ito et al., 2005). Therefore, these considerations offer an explanation to the apparent discrepancy between the steady-state measurements by NMR implying a near complete oxidation of glucose during activation (Lin et al., 2012; Mangia et al., 2007a; Schaller et al., 2013) and PET (Fox and Raichle, 1986; Ito et al., 2005).

Nevertheless, numerous studies have reported different experimental measurements of $\Delta CBF/\Delta CMR_{O2}$ mismatch in human brain (reviewed in Buxton (2010); Hyder (2004); Hyder and Rothman (2012)). The original $\Delta CBF/\Delta CMR_{O2}$ ~6 reported by Fox and Raichle (Fox and Raichle, 1986) is generally higher than other human brain PET studies (Hyder, 2004; Ito et al., 2005; Kuwabara et al., 1992; Marrett and Gjedde, 1997). For calibrated BOLD-measurement studies, the ratio $\Delta CBF/\Delta CMR_{O2}$ generally lies from 2 to 4 (Buxton, 2010). In animal studies, large CMR_{O2} and CBF changes were observed during sensory stimulation in anesthetized rats (reviewed in Hyder and Rothman (2012)). Additionally, ^{13}C MRS studies (in animal and human) allows the correlation between neuronal glucose oxidation and neuronal activity, and revealed high oxidative metabolism demand during neuronal activation (Chen et al., 2001; Chhina et al., 2001; Hyder et al., 1996, 1997). In vivo ^{17}O NMR may also be used to directly and non-invasively determine CMR_{O2} (Mateescu, 2003; Zhu and Chen, 2011; Zhu et al., 2005) with high reliability and reproducibility (Zhu et al., 2007), as well as the simultaneous in vivo measurements of CBF (Zhu et al., 2013), which may help unraveling the role of oxidative metabolism during functional activity.

These human and animal studies suggest that the mismatch ratio and general glucose metabolism may depend on many criteria such as: age of the subject (Kalpouzos et al., 2009; Nelhig, 1997), brain regions, methodology, stimulus frequency (Vafaee and Gjedde, 2000; Vafaee et al., 1999) and duration (Herman et al., 2009; Mintun et al., 2002), basal metabolic status (Shen et al., 2008; Sicard and Duong, 2005) and the use of anesthesia (Austin et al., 2005; Dienel, 2012; Kim et al., 2010). Finally, (Dienel, 2012) reviewed that different stimulus paradigm increase CMR_{Glc} with different rates. The various reports, mainly from brain imaging and spectroscopy methods, contribute to a better understanding of brain functions at rest and during neural activation, but also paint a complex picture that is complicated to quantitatively estimate.

It is important to stress that although the above considerations imply a transient mismatch in CMR_{Glc} and CMR_{O2}, this does not imply an uncoupling of glucose and oxygen metabolism. Rather these events are likely coordinated, as Glu is an integrated element of the malate–aspartate shuttle (McKenna et al., 2006), critical in regulating cytosolic redox potential. In other words, we propose that, in order to achieve the new metabolic steady state, glycolysis must transiently increase above CMR_{O2}, which is most likely the result of coupled metabolic events. However, the conclusion by Mangia et al. (2007a), namely that activation is primarily powered by increased ATP production produced by oxidative metabolism, is maintained.

We conclude that this study reports lactate and glutamate increases in the motor cortex, which reached a new steady state after 1–2 min of activation. The observed metabolite changes were similar to those reported in previous studies in the visual cortex at high field (Lin et al., 2012; Mangia et al., 2007a; Schaller et al., 2013). We also infer that the small but significant increases in Glu and Lac are most likely a general manifestation of neuronal activation powered at steady-state mainly by oxidative metabolism. However, initially an increase in ΔCMR_{O2} that is transiently below that of ΔCMR_{Glc} in the first 1–2 min of activation is stipulated.

Acknowledgments

This work was supported by the Centre d'Imagerie Bio-Médicale (CIBM) of the University of Lausanne (UNIL), the Swiss Federal Institute of Technology Lausanne (EPFL), the University of Geneva (UniGe), the Centre Hospitalier Universitaire Vaudois (CHUV), the Hôpitaux Universitaires de Genève (HUG) and the Leenaards and the Jeantet Foundations and by a SNF grant No 131087 to R. Gruetter.

Conflict of interest

The authors declare no conflict of interest.

References

Alkire, M.T., Pomfrett, C.J., Haier, R.J., Gianzero, M.V., Chan, C.M., Jacobsen, B.P., Fallon, J.H., 1999. Functional brain imaging during anesthesia in humans: effects of halothane on global and regional cerebral glucose metabolism. Anesthesiology 90, 701–709.

Austin, V.C., Blamire, A.M., Allers, K.A., Sharp, T., Styles, P., Matthews, P.M., Sibson, N.R., 2005. Confounding effects of anesthesia on functional activation in rodent brain: a study of halothane and alpha-chloralose anesthesia. Neuroimage 24, 92–100.

Boucard, C.C., Mostert, J.P., Cornelissen, F.W., De Keyser, J., Oudkerk, M., Sijens, P.E., 2005. Visual stimulation, ^{1}H MR spectroscopy and fMRI of the human visual pathways. Eur. Radiol. 15, 47–52.

Branzoli, F., Techawiboonwong, A., Kan, H., Webb, A., Ronen, I., 2013. Functional diffusion-weighted magnetic resonance spectroscopy of the human primary visual cortex at 7 T. Magn. Reson. Med. 69, 303–309.

Buxton, R.B., 2010. Interpreting oxygenation-based neuroimaging signals: the importance and the challenge of understanding brain oxygen metabolism. Front. Neuroenerg. 2, 8.

Chen, W., Novotny, E.J., Zhu, X.H., Rothman, D.L., Shulman, R.G., 1993. Localized ^{1}H NMR measurement of glucose consumption in the human brain during visual stimulation. Proc. Natl. Acad. Sci. U. S. A. 90, 9896–9900.
Chen, W., Zhu, X.H., Gruetter, R., Seaquist, E.R., Adriany, G., Ugurbil, K., 2001. Study of tricarboxylic acid cycle flux changes in human visual cortex during hemifield visual stimulation using (1)H–[(13)C] MRS and fMRI. Magn. Reson. Med. 45, 349–355.
Chhina, N., Kuestermann, E., Halliday, J., Simpson, L.J., Macdonald, I.A., Bachelard, H.S., Morris, P.G., 2001. Measurement of human tricarboxylic acid cycle rates during visual activation by (13)C magnetic resonance spectroscopy. J. Neurosci. Res. 66, 737–746.
Christ, A., Kainz, W., Hahn, E.G., Honegger, K., Zefferer, M., Neufeld, E., Rascher, W., Janka, R., Bautz, W., Chen, J., Kiefer, B., Schmitt, P., Hollenbach, H.P., Shen, J., Oberle, M., Szczerba, D., Kam, A., Guag, J.W., Kuster, N., 2010. The virtual family—development of surface-based anatomical models of two adults and two children for dosimetric simulations. Phys. Med. Biol. 55, N23–N38.
Davis, T.L., Kwong, K.K., Weisskoff, R.M., Rosen, B.R., 1998. Calibrated functional MRI: mapping the dynamics of oxidative metabolism. Proc. Natl. Acad. Sci. U. S. A. 95, 1834–1839.
Dienel, G.A., 2012. Fueling and imaging brain activation. ASN Neuro. 4 (5), 267–321.
Eggenschwiler, F., Kober, T., Magill, A.W., Gruetter, R., Marques, J.P., 2011. SA2RAGE: a new sequence for fast B(1) (+)-mapping. Magn. Reson. Med. 67 (6), 1609–1619.
Fox, P.T., Raichle, M.E., 1986. Focal physiological uncoupling of cerebral blood flow and oxidative metabolism during somatosensory stimulation in human subjects. Proc. Natl. Acad. Sci. U. S. A. 83, 1140–1144.
Fox, P.T., Raichle, M.E., Mintun, M.A., Dence, C., 1988. Nonoxidative glucose consumption during focal physiologic neural activity. Science 241, 462–464.
Frahm, J., Kruger, G., Merboldt, K.D., Kleinschmidt, A., 1996. Dynamic uncoupling and recoupling of perfusion and oxidative metabolism during focal brain activation in man. Magn. Reson. Med. 35, 143–148.
Fujita, H., Kuwabara, H., Reutens, D.C., Gjedde, A., 1999. Oxygen consumption of cerebral cortex fails to increase during continued vibrotactile stimulation. J. Cereb. Blood Flow Metab. 19, 266–271.
Gjedde, A., Marrett, S., Vafaee, M., 2002. Oxidative and nonoxidative metabolism of excited neurons and astrocytes. J. Cereb. Blood Flow Metab. 22, 1–14.
Govindaraju, V., Young, K., Maudsley, A.A., 2000. Proton NMR chemical shifts and coupling constants for brain metabolites. NMR Biomed. 13, 129–153.
Gruetter, R., 1993. Automatic, localized in vivo adjustment of all first- and second-order shim coils. Magn. Reson. Med. 29, 804–811.
Gruetter, R., Tkac, I., 2000. Field mapping without reference scan using asymmetric echo-planar techniques. Magn. Reson. Med. 43, 319–323.
Hawkins, R.A., Miller, A.L., Nielsen, R.C., Veech, R.L., 1973. The acute action of ammonia on rat brain metabolism in vivo. Biochem. J. 134, 1001–1008.
Herman, P., Sanganahalli, B.G., Blumenfeld, H., Hyder, F., 2009. Cerebral oxygen demand for short-lived and steady-state events. J. Neurochem. 109 (Suppl. 1), 73–79.
Hoge, R.D., Atkinson, J., Gill, B., Crelier, G.R., Marrett, S., Pike, G.B., 1999. Linear coupling between cerebral blood flow and oxygen consumption in activated human cortex. Proc. Natl. Acad. Sci. U. S. A. 96, 9403–9408.
Huisman, M.C., van Golen, L.W., Hoetjes, N.J., Greuter, H.N., Schober, P., Ijzerman, R.G., Diamant, M., Lammertsma, A.A., 2012. Cerebral blood flow and glucose metabolism in healthy volunteers measured using a high-resolution PET scanner. EJNMMI Res. 2, 63.
Hyder, F., 2004. Neuroimaging with calibrated FMRI. Stroke 35, 2635–2641.
Hyder, F., Rothman, D.L., 2012. Quantitative fMRI and oxidative neuroenergetics. Neuroimage 62, 985–994.
Hyder, F., Chase, J.R., Behar, K.L., Mason, G.F., Siddeek, M., Rothman, D.L., Shulman, R.G., 1996. Increased tricarboxylic acid cycle flux in rat brain during forepaw stimulation detected with ^{1}H[^{13}C]NMR. Proc. Natl. Acad. Sci. U. S. A. 93, 7612–7617.
Hyder, F., Rothman, D.L., Mason, G.F., Rangarajan, A., Behar, K.L., Shulman, R.G., 1997. Oxidative glucose metabolism in rat brain during single forepaw stimulation: a spatially localized ^{1}H[^{13}C] nuclear magnetic resonance study. J. Cereb. Blood Flow Metab. 17, 1040–1047.
Ito, H., Ibaraki, M., Kanno, I., Fukuda, H., Miura, S., 2005. Changes in cerebral blood flow and cerebral oxygen metabolism during neural activation measured by positron emission tomography: comparison with blood oxygenation level-dependent contrast measured by functional magnetic resonance imaging. J. Cereb. Blood Flow Metab. 25, 371–377.
Kalpouzos, G., Chetelat, G., Baron, J.C., Landeau, B., Mevel, K., Godeau, C., Barre, L., Constans, J.M., Viader, F., Eustache, F., Desgranges, B., 2009. Voxel-based mapping of brain gray matter volume and glucose metabolism profiles in normal aging. Neurobiol. Aging 30, 112–124.
Kim, S.G., Ugurbil, K., 1997. Comparison of blood oxygenation and cerebral blood flow effects in fMRI: estimation of relative oxygen consumption change. Magn. Reson. Med. 38, 59–65.
Kim, S.G., Rostrup, E., Larsson, H.B., Ogawa, S., Paulson, O.B., 1999. Determination of relative CMRO2 from CBF and BOLD changes: significant increase of oxygen consumption rate during visual stimulation. Magn. Reson. Med. 41, 1152–1161.
Kim, T., Masamoto, K., Fukuda, M., Vazquez, A., Kim, S.G., 2010. Frequency-dependent neural activity, CBF, and BOLD fMRI to somatosensory stimuli in isoflurane-anesthetized rats. Neuroimage 52, 224–233.
Kuwabara, H., Ohta, S., Brust, P., Meyer, E., Gjedde, A., 1992. Density of perfused capillaries in living human brain during functional activation. Prog. Brain Res. 91, 209–215.
Kuwabara, T., Watanabe, H., Tsuji, S., Yuasa, T., 1995. Lactate rise in the basal ganglia accompanying finger movements: a localized 1H-MRS study. Brain Res. 670, 326–328.
Lin, A.L., Fox, P.T., Hardies, J., Duong, T.Q., Gao, J.H., 2010. Nonlinear coupling between cerebral blood flow, oxygen consumption, and ATP production in human visual cortex. Proc. Natl. Acad. Sci. U. S. A. 107, 8446–8451.
Lin, Y., Stephenson, M.C., Xin, L., Napolitano, A., Morris, P.G., 2012. Investigating the metabolic changes due to visual stimulation using functional proton magnetic resonance spectroscopy at 7 T. J. Cereb. Blood Flow Metab. 32 (8), 1484–1495.
Liu, Z.M., Schmidt, K.F., Sicard, K.M., Duong, T.Q., 2004. Imaging oxygen consumption in forepaw somatosensory stimulation in rats under isoflurane anesthesia. Magn. Reson. Med. 52, 277–285.
Mangia, S., Tkac, I., Gruetter, R., Van de Moortele, P.F., Maraviglia, B., Ugurbil, K., 2007a. Sustained neuronal activation raises oxidative metabolism to a new steady-state level: evidence from ^{1}H NMR spectroscopy in the human visual cortex. J. Cereb. Blood Flow Metab. 27, 1055–1063.
Mangia, S., Tkac, I., Logothetis, N.K., Gruetter, R., Van de Moortele, P.F., Ugurbil, K., 2007b. Dynamics of lactate concentration and blood oxygen level-dependent effect in the human visual cortex during repeated identical stimuli. J. Neurosci. Res. 85, 3340–3346.
Mangia, S., Giove, F., Dinuzzo, M., 2012. Metabolic pathways and activity-dependent modulation of glutamate concentration in the human brain. Neurochem. Res. 37, 2554–2561.
Marques, J.P., Kober, T., Krueger, G., van der Zwaag, W., Van de Moortele, P.F., Gruetter, R., 2010. MP2RAGE, a self bias-field corrected sequence for improved segmentation and T1-mapping at high field. Neuroimage 49, 1271–1281.
Marrett, S., Gjedde, A., 1997. Changes of blood flow and oxygen consumption in visual cortex of living humans. Adv. Exp. Med. Biol. 413, 205–208.
Mateescu, G.D., 2003. Functional oxygen-17 magnetic resonance imaging and localized spectroscopy. Adv. Exp. Med. Biol. 510, 213–218.
McKenna, M.C., Stevenson, J.H., Huang, X., Hopkins, I.B., 2000. Differential distribution of the enzymes glutamate dehydrogenase and aspartate aminotransferase in cortical synaptic mitochondria contributes to metabolic compartmentation in cortical synaptic terminals. Neurochem. Int. 37, 229–241.
McKenna, M.C., Waagepetersen, H.S., Schousboe, A., Sonnewald, U., 2006. Neuronal and astrocytic shuttle mechanisms for cytosolic-mitochondrial transfer of reducing equivalents: current evidence and pharmacological tools. Biochem. Pharmacol. 71, 399–407.
Mekle, R., Mlynarik, V., Gambarota, G., Hergt, M., Krueger, G., Gruetter, R., 2009. MR spectroscopy of the human brain with enhanced signal intensity at ultrashort echo times on a clinical platform at 3 T and 7 T. Magn. Reson. Med. 61, 1279–1285.
Merboldt, K.D., Bruhn, H., Hanicke, W., Michaelis, T., Frahm, J., 1992. Decrease of glucose in the human visual cortex during photic stimulation. Magn. Reson. Med. 25, 187–194.
Mintun, M.A., Vlassenko, A.G., Shulman, G.L., Snyder, A.Z., 2002. Time-related increase of oxygen utilization in continuously activated human visual cortex. Neuroimage 16, 531–537.
Nelhig, A., 1997. Cerebral energy metabolism, glucose transport and blood flow: changes with maturation and adaptation to hypoglycaemia. Diabetes Metab. 23, 18–29.
Oz, G., Berkich, D.A., Henry, P.G., Xu, Y., LaNoue, K., Hutson, S.M., Gruetter, R., 2004. Neuroglial metabolism in the awake rat brain: CO2 fixation increases with brain activity. J. Neurosci. 24, 11273–11279.
Paulson, O.B., Hasselbalch, S.G., Rostrup, E., Knudsen, G.M., Pelligrino, D., 2010. Cerebral blood flow response to functional activation. J. Cereb. Blood Flow Metab. 30, 2–14.
Prichard, J., Rothman, D., Novotny, E., Petroff, O., Kuwabara, T., Avison, M., Howseman, A., Hanstock, C., Shulman, R., 1991. Lactate rise detected by ^{1}H NMR in human visual cortex during physiologic stimulation. Proc. Natl. Acad. Sci. U. S. A. 88, 5829–5831.
Provencher, S.W., 1993. Estimation of metabolite concentrations from localized *in vivo* proton NMR spectra. Magn. Reson. Med. 30, 672–679.
Rothman, D.L., Behar, K.L., Hyder, F., Shulman, R.G., 2003. In vivo NMR studies of the glutamate neurotransmitter flux and neuroenergetics: implications for brain function. Annu. Rev. Physiol. 65, 401–427.
Sandor, P.S., Dydak, U., Schoenen, J., Kollias, S.S., Hess, K., Boesiger, P., Agosti, R.M., 2005. MR-spectroscopic imaging during visual stimulation in subgroups of migraine with aura. Cephalalgia 25, 507–518.
Sappey-Marinier, D., Calabrese, G., Fein, G., Hugg, J.W., Biggins, C., Weiner, M.W., 1992. Effect of photic stimulation on human visual cortex lactate and phosphates using ^{1}H and 31P magnetic resonance spectroscopy. J. Cereb. Blood Flow Metab. 12, 584–592.
Schaller, B., Mekle, R., Xin, L., Kunz, N., Gruetter, R., 2013. Net increase of lactate and glutamate concentration in activated human visual cortex detected with magnetic resonance spectroscopy at 7 Tesla. J. Neurosci. Res. 91 (8), 1076–1083.
Shen, Q., Ren, H., Duong, T.Q., 2008. CBF, BOLD, CBV, and CMRO(2) fMRI signal temporal dynamics at 500-msec resolution. J. Magn. Reson. Imaging 27, 599–606.
Sicard, K.M., Duong, T.Q., 2005. Effects of hypoxia, hyperoxia, and hypercapnia on baseline and stimulus-evoked BOLD, CBF, and CMRO2 in spontaneously breathing animals. Neuroimage 25, 850–858.
Siesjo, B.K., 1978. In: Wiley (Ed.), Brain Energy Metabolism, New-York, pp. 101–110.
Snaar, J.E., Teeuwisse, W.M., Versluis, M.J., van Buchem, M.A., Kan, H.E., Smith, N.B., Webb, A.G., 2011. Improvements in high-field localized MRS of the medial temporal lobe in humans using new deformable high-dielectric materials. NMR Biomed. 24, 873–879.
Teeuwisse, W.M., Brink, W.M., Haines, K.N., Webb, A.G., 2012a. Simulations of high permittivity materials for 7 T neuroimaging and evaluation of a new barium titanate-based dielectric. Magn. Reson. Med. 67, 912–918.
Teeuwisse, W.M., Brink, W.M., Webb, A.G., 2012b. Quantitative assessment of the effects of high-permittivity pads in 7 Tesla MRI of the brain. Magn. Reson. Med. 67, 1285–1293.
Tkac, I., Gruetter, R., 2005. Methodology of H NMR Spectroscopy of the Human Brain at Very High Magnetic Fields. Appl. Magn. Reson. 29, 139–157.
Tkac, I., Andersen, P., Adriany, G., Merkle, H., Ugurbil, K., Gruetter, R., 2001. *In vivo* ^{1}H NMR spectroscopy of the human brain at 7 T. Magn. Reson. Med. 46, 451–456.
Tkac, I., Oz, G., Adriany, G., Ugurbil, K., Gruetter, R., 2009. *In vivo* ^{1}H NMR spectroscopy of the human brain at high magnetic fields: metabolite quantification at 4 T vs. 7 T. Magn. Reson. Med. 62, 868–879.

Vafaee, M.S., Gjedde, A., 2000. Model of blood–brain transfer of oxygen explains nonlinear flow-metabolism coupling during stimulation of visual cortex. J. Cereb. Blood Flow Metab. 20, 747–754.
Vafaee, M.S., Gjedde, A., 2004. Spatially dissociated flow-metabolism coupling in brain activation. Neuroimage 21, 507–515.
Vafaee, M.S., Meyer, E., Marrett, S., Paus, T., Evans, A.C., Gjedde, A., 1999. Frequency-dependent changes in cerebral metabolic rate of oxygen during activation of human visual cortex. J. Cereb. Blood Flow Metab. 19, 272–277.
Vafaee, M.S., Vang, K., Bergersen, L.H., Gjedde, A., 2012. Oxygen consumption and blood flow coupling in human motor cortex during intense finger tapping: implication for a role of lactate. J. Cereb. Blood Flow Metab. 32, 1859–1868.
van der Zwaag, W., Marques, J.P., Hergt, M., Gruetter, R., 2009. Investigation of high-resolution functional magnetic resonance imaging by means of surface and array radiofrequency coils at 7 T. Magn. Reson. Imaging 27, 1011–1018.
Wey, H.Y., Wang, D.J., Duong, T.Q., 2011. Baseline CBF, and BOLD, CBF, and CMRO2 fMRI of visual and vibrotactile stimulations in baboons. J. Cereb. Blood Flow Metab. 31, 715–724.
Xin, L., Gambarota, G., Mlynarik, V., Gruetter, R., 2008. Proton T2 relaxation time of J-coupled cerebral metabolites in rat brain at 9.4 T. NMR Biomed. 21, 396–401.
Xin, L., Schaller, B., Mlynarik, V., Lu, H., Gruetter, R., 2012. Proton T(1) relaxation times of metabolites in human occipital white and gray matter at 7 T. Magn. Reson. Med. 69 (4), 931–936.
Zhu, X.H., Chen, W., 2001. Observed BOLD effects on cerebral metabolite resonances in human visual cortex during visual stimulation: a functional (1)H MRS study at 4 T. Magn. Reson. Med. 46, 841–847.
Zhu, X.H., Chen, W., 2011. *In vivo* oxygen-17 NMR for imaging brain oxygen metabolism at high field. Prog. Nucl. Magn. Reson. Spectrosc. 59, 319–335.
Zhu, X.H., Zhang, N., Zhang, Y., Zhang, X., Ugurbil, K., Chen, W., 2005. *In vivo* 17O NMR approaches for brain study at high field. NMR Biomed. 18, 83–103.
Zhu, X.H., Zhang, Y., Zhang, N., Ugurbil, K., Chen, W., 2007. Noninvasive and three-dimensional imaging of CMRO(2) in rats at 9.4 T: reproducibility test and normothermia/hypothermia comparison study. J. Cereb. Blood Flow Metab. 27, 1225–1234.
Zhu, X.H., Zhang, N., Zhang, Y., Ugurbil, K., Chen, W., 2009. New insights into central roles of cerebral oxygen metabolism in the resting and stimulus-evoked brain. J. Cereb. Blood Flow Metab. 29, 10–18.
Zhu, X.H., Chen, J.M., Tu, T.W., Chen, W., Song, S.K., 2013. Simultaneous and noninvasive imaging of cerebral oxygen metabolic rate, blood flow and oxygen extraction fraction in stroke mice. Neuroimage 64, 437–447.